

Magneto-Elastic Effect in Non-Newtonian Ferrofluid Droplets Impacting Superhydrophobic Surfaces

Gudlavalleti V V S Vara Prasad, Purbarun Dhar,* and Devranjan Samanta*



Cite This: *Langmuir* 2021, 37, 9673–9682



Read Online

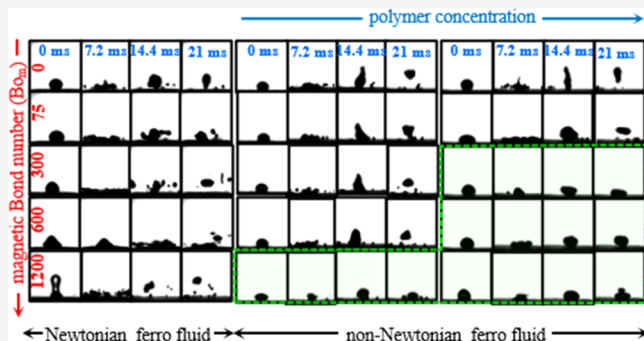
ACCESS |

Metrics & More

Article Recommendations

Supporting Information

ABSTRACT: In this article, we propose, with the aid of detailed experiments and scaling analysis, the existence of magneto-elastic effects in the impact hydrodynamics of non-Newtonian ferrofluid droplets on superhydrophobic surfaces in the presence of a magnetic field. The effects of magnetic Bond number (Bo_m), Weber number (We), polymer concentration, and magnetic nanoparticle (Fe_3O_4) concentration in the ferrofluids were investigated. In comparison to Newtonian ferrofluid droplets, addition of polymers caused rebound suppression of the droplets relatively at lower Bo_m for a fixed magnetic nanoparticle concentration and We . We further observed that for a fixed polymer concentration and We , increasing magnetic nanoparticle concentration also triggers earlier rebound suppression with increasing Bo_m . In the absence of the magnetic nanoparticles, the non-Newtonian droplets do not show rebound suppression for the range of Bo_m investigated. Likewise, the Newtonian ferrofluids show rebound suppression at large Bo_m . This intriguing interplay of elastic effects of polymer chains and the magnetic nanoparticles, dubbed as the magneto-elastic effect, is noted to lead to the rebound suppression. We establish a scaling relationship to show that the rebound suppression is observed as a manifestation of the onset of magneto-elastic instability only when the proposed magnetic Weissenberg number (Wi_m) exceeds unity. We also put forward a phase map to identify the various regimes of impact ferrohydrodynamics of such droplets and the occurrence of the magneto-elastic effect.



1. INTRODUCTION

The dynamics and phenomenology of droplet impact on a solid or liquid surface are scientifically important due to the wide range of associated applications. Droplet impact dynamics comprises various physical phenomena, like deposition, rebound, partial rebound,¹ splashing, and fragmentation. Understanding the dynamics is a decisive factor in many applications like inkjet printing,² spray coating and painting, spray cooling, and retention of pesticide sprays on vegetation to prevent groundwater contamination, pesticide over-use, and so forth. The manipulation of impact dynamics of ferrofluid droplets by a magnetic field can lead to significant improvements in magnetic 3D printing³ performance and may also promote control of shape distortions in metallic droplets during welding or soldering. The magnetic force on ferrofluid droplets is important for handling magnetic beads, manipulating ferrofluid droplet transport, and splitting in microfluidic devices.⁴ Ahmed et al.⁵ studied the maximum spreading dynamics of a ferrofluid droplet under the effect of vertically oriented magnetic field. The maximum spreading of the droplet was proportional to the corresponding non-dimensional numbers, like Weber number (We), magnetic Bond number (Bo_m), and Reynolds number (Re).

Sudo et al.⁶ explored the effect of the magnetic field on the maximum spreading diameter and spike formation within the liquid lamella of impacting magnetic fluid droplets. Rahimi and Weihs⁷ reported the droplet impact dynamics of magneto-rheological fluids and the dependence of the maximum spreading factor on the magnetic field strength and Reynolds number (Re). Zhou and Jing⁸ showed how a magnetic field affects the collision characteristics, oscillation kinetics, maximum spreading factor, maximum recoiling height, and the retraction height of ferrofluid droplets for different impact velocities. Sahoo et al.⁹ experimentally investigated impact dynamics of ferrofluid droplets on superhydrophobic (SH) surfaces under the influence of the horizontal magnetic field and reported that significant rebound suppression phenomena was observed at moderate magnetic Bond numbers ($Bo_m \sim 300$). The ferrofluid droplet liquid lamella was shown to

Received: March 31, 2021

Revised: July 16, 2021

Published: August 5, 2021



become largely unstable due to nucleation of holes during the retraction stage at higher magnetic Bond numbers ($Bo_m > 300$), leading to distinct fragmentation kinetics fairly uncommon in the droplet impact literature.

In recent years, elastic and viscoelastic effects during impact dynamics of non-Newtonian fluid droplets have gathered attention due to the observation of rebound suppression on SH surfaces.^{10–13} It was shown that addition of minute amounts of flexible, very long-chain polymers like polyethylene oxide (PEO) or polyacrylamide (PAM) to water arrests the droplet rebound on SH surfaces. Initially, it was believed to be due to the higher energy dissipation caused by the elongational viscosity of the polymer solutions. Bartolo et al.¹⁰ proposed that during retraction, the polymer chains generate a large amount of normal stresses and slow down the moving contact line of the droplet. This opposes the capillary force and retraction kinetic energy, which ultimately leads to rebound suppression. Mao et al.¹¹ showed the dependence of rebound behavior on the spread factor and the static contact angle of the droplet. Smith and Bertola¹² showed the extensional deformation of solvated fluorescent-dyed DNA molecules near the receding contact line of a droplet slows down the retraction process.

Later, Dhar et al.¹³ showed the governing roles of the impact velocity and polymer concentrations as critical parameters to determine the onset of rebound suppression. Based on the shear rate during onset of retraction and the relaxation time scale of the elastic fluid, they showed that the onset of rebound suppression occurs only under circumstances where the governing Weissenberg number (Wi) exceeds one. They further showed that the change in retraction dynamics of the non-Newtonian droplets can also be used to morph the thermo-species transport behavior, such as delaying the droplet Leidenfrost effect.¹⁴ Zang et al.¹⁵ observed a transition from droplet rebound to sticking by the addition of PEO to Newtonian fluids and reported the importance of sliding angle of the fluid droplet, in addition to the contact angle. Yun et al.¹⁶ reported the effect of the electric field on non-axisymmetric droplets toward inhibiting droplet rebound and also investigated the impact dynamics of ellipsoidal drops as a function of the geometric aspect ratio and impact Weber number.¹⁷ Antonini et al.¹⁸ showed the importance of the receding contact angle of the rebounding droplet on hydrophobic and SH surfaces. Very recently, a study revisited the role of elongational viscosity on rebound suppression event using advanced experimental techniques like total internal reflection microscopy.¹⁹

In this article, we have explored a novel phenomenon in non-Newtonian ferrofluid droplets, which may be given a nomenclature of magneto-elastic effects. We have investigated the impact and rebound dynamics of polymer solution-based ferrofluid droplets under the influence of a horizontal magnetic field and the phenomenology of onset of conjugated magnetic and elastic instability, leading to suppressed droplet rebound. The impact of magneto-hydrodynamics of the droplet has been characterized by four dimensionless parameters, viz. the Weber number ($We = \rho V_0^2 D_0 / \sigma_{lv}$, defined as the ratio of inertial force to surface tension force), the magnetic Bond number ($Bo_m = B^2 D_0 / \mu_0 \sigma_{lv}$, defined as the ratio of magnetic force to surface tension force), the magnetic capillary number ($Ca_m = \eta V_0 / \sigma_{lv}$, defined as the ratio of viscous force to surface tension forces under influence of the magnetic field), and the Hartmann number ($Ha = \rho m B D_0 / 2 V_0 \eta$,²⁰ defined as the ratio of magnetic

force to viscous force). Here, ρ , V_0 , D_0 , σ_{lv} , B , m , μ_0 , and η denote the density, impact velocity, pre-impact diameter, surface tension, magnetic flux density, magnetic moment per unit mass, magnetic permeability of free space, and viscosity of the ferrofluid droplet, respectively. Furthermore, we theorize and show that the onset of suppression of droplet rebound depends on the magneto-elastic effect, which is a conjugation of the polymer relaxation time, the shear rate at the contact line during the retraction stage, and the ferrohydrodynamics of the droplet. We have also highlighted the critical role of a proposed magnetic Weissenberg number in governing the onset criterion for droplet rebound suppression.

2. MATERIALS AND METHODOLOGIES

2.1. Non-Newtonian Ferrofluids. The ferrofluids were synthesized using iron(II,III) oxide (Fe_3O_4) nanoparticles (Alfa Aesar India, > 98.5% purity) of average particle diameter 20–30 nm [noted from scanning electron microscopy images (not illustrated)]. Polyethylene glycol (PEG 400, analytical grade, Finar Chemicals, India) was used to render the ferrofluids non-Newtonian. Initially, polymer solutions using PEG and deionized (DI) water were synthesized (5 and 10% v/v of PEG). To these non-Newtonian fluids, the Fe_3O_4 nanoparticles are dispersed (2.5 and 5 wt %) and stabilized following a similar reported protocol.²¹ The polymeric ferrofluids were subjected to ultra-sonication for 2 h to ensure colloidal stability. We adopt a nomenclature method for the polymeric ferrofluids: a sample containing “x” % PEG in water and “y” % Fe_3O_4 particles is written as Px–Fy. Thus, the sample P5–F2.5 contains 5% v/v PEG in water with 2.5 w/w % particles dispersed in it. Any sample with P0 signifies Newtonian ferrofluid.

2.2. Substrates. Glass slides coated with a commercial SH coating (Neverwet Ultra Ever dry, USA) were used as substrates in the experimental study. The substrates were prepared by following a previously reported protocol.²² Before spray coating, each glass slide was cleaned with DI water followed by acetone and oven-dried thoroughly. The static equilibrium contact angles of the ferrofluid droplets are shown in Figure S1 (refer Supporting Information). The static contact angle of non-Newtonian ferrofluid droplets on the SH surface is in the range of 155 ± 30 . The surface tension of the ferrofluids (refer Supporting Information, Table S1) was measured using the pendant drop method, and the equilibrium static contact angles were measured from image analysis. The surface tension values were noted to be minimally altered due to the magnetic field and in the range of 76 ± 3 mN/m.

2.3. Experimental Setup. The overall arrangement of the experimental setup is shown in Figure 1. A digitized droplet dispensing mechanism (DDM) unit ($\pm 0.1 \mu L$ volumetric accuracy) was used to dispense droplets of fixed volume, via a glass micro-syringe with a flat head steel needle (22 gauge). The impact height of the droplet was adjusted to obtain different impact velocities and different We . The droplet was allowed to fall freely on the substrate, which was placed between the poles of an electromagnet. An electromagnet (Holmarc Opto-Mechtronics Ltd., India) was used to generate the magnetic field, with controlled field strengths of 0–0.2 T. The field strength varied by changing current input across the electromagnet pole windings using a direct current power supply (Polytonic Corp., India) unit. Flat face cylindrical iron billets of diameter 100 mm act as the magnetic pole shoes. The magnetic field strength near the substrate was calibrated by a Gauss meter (Holmarc Opto-Mechtronics Ltd., India) for different current inputs to the pole windings. Beyond 0.2 T, the free falling droplet shape is distorted by the field before impact, which induces artefacts to the post impact hydrodynamics. Accordingly, the experiments have been restricted to 0.2 T.

The micro-syringe needle and SH slides were positioned at the center of the electromagnet poles to ensure that the droplet impact was in a uniform magnetic field. The schematic of the front and top views of positioning of the droplet and the associated coordinate

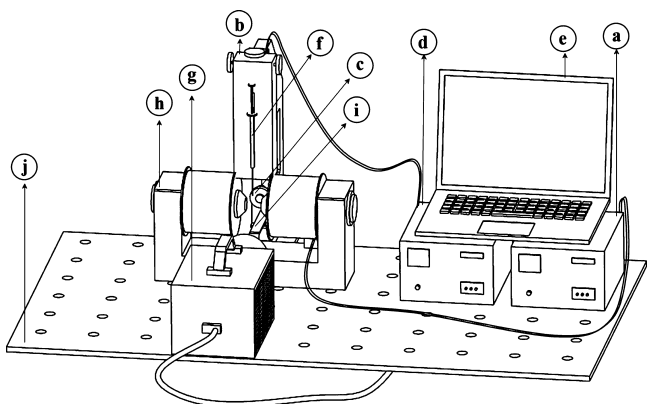


Figure 1. Schematic of the experimental setup. (a) Electromagnet power controller, (b) DDM unit, (c) LED array for backlight illumination, (d) DDM and LED array intensity controller, (e) computer for data acquisition and camera control, (f) micro-syringe, (g) high speed camera, (h) programmable electromagnet unit, (i) spray-coated SH surface, and (j) bread board.

frame of reference are illustrated in Figure S2 (*Supporting Information*). The droplet dynamics was recorded with a high-speed camera (Fastcam SA4, Photron, UK) attached with a macro lens of constant focal length of 105 mm (Nikkor, Nikon). All experiments were conducted at 3600 frames per second and 1024×1024 pixel resolution. For backlight illumination, an intensity-controlled LED array was used. Rheological tests of the fluids were performed using a rotational rheometer (Anton Paar, Germany). A plate and plate geometry (PP-20) attached to a magnetorheological module is used to determine the shear viscosity (η), elastic modulus (G'), and viscous modulus (G'') (refer Figures S3 and S4 in *Supporting Information*) under the influence of the magnetic field. All tests and experiments were repeated thrice to check for repeatability.

3. RESULTS AND DISCUSSION

3.1. Droplet Impact Ferrohydrodynamics. We start the discussion with the ferrohydrodynamics of the droplet impact event on SH surfaces. Figure 2a–c shows the effect of the magnetic Bond number on the ferrofluid droplet spreading due to increasing non-Newtonian nature (achieved by increasing polymer concentrations) at $We \sim 100$. In both Newtonian (water-based) and non-Newtonian (polymer solution-based)

ferrofluid droplet cases, the droplet spreads with radial symmetry intact in the absence of the magnetic field ($Bo_m = 0$). For the Newtonian case (P0–F2.5), the droplets spread to a larger extent along the z -direction compared to the x -direction (refer Figure 2c, first row, first column for the coordinate axis) with increasing magnetic Bond number (Bo_m) (Figure 2a). This is due to the interplay between magnetic forces and the surface tension force and has been discussed in detail in our previous report.⁹ As the droplet spreads in the presence of the magnetic field, the rate of change of the magnetic force on the droplet increases. Lenz's law, which suppresses the cause of change in the magnetic force in the system, thereby opposes the spread in the x -direction, while the droplet spreads unrestrictedly along the z -direction. Additionally, the liquid film formed and enclosed by the spreading rim (Figure 2a, 4th row, 3rd column) undergoes rupture due to nucleation and proliferation of holes at high values of magnetic Bond number (at $Bo_m \sim 1200$).⁹ We have discussed the genesis of the rupturing instability from energy conservation considerations in the previous report.⁹ Now we shift the focus to the non-Newtonian ferrofluids. The impact phenomenon is characterized by the formation of distinct filaments. This can be observed from Figure 2b,c. With increase in either polymer concentration or the Bo_m , the rupturing instability of the spread droplet is noted to be seized. Also, the asymmetric elongation along the z -direction is notably pronounced, similar to the Newtonian drop impact dynamics in the presence of the magnetic field.⁹

To quantify the asymmetric spreading kinetics, we define the maximum non-dimensional orthogonal spreading ratio as $\xi_{\max} = (D_z/D_x)_{\max}$ and illustrate the same in Figure 3. Figure 3 illustrates the non-dimensional orthogonal maximum spreading ratio ξ_{\max} for both Newtonian and non-Newtonian ferrofluid droplets for varied magnetic field intensity, quantified through the magnetic Bond number such as 0 T ($Bo_m = 0$), 0.05 T ($Bo_m \sim 75$), 0.10 T ($Bo_m \sim 600$), and 0.20 T ($Bo_m \sim 1200$). Figure 3a shows the effect of Bo_m with varying polymer concentrations on the ξ_{\max} . Initially, the ξ_{\max} increases linearly with Bo_m (~ 75) and then saturates to an almost constant value. It must be noted that the saturated value of ξ_{\max} is increasing with the increase of polymer concentrations. One of the potential reason for the initial linear increase of ξ_{\max} with Bo_m

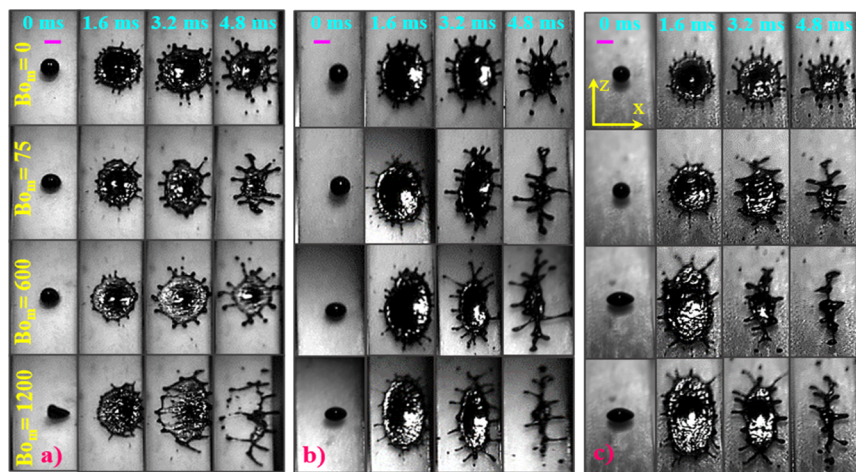


Figure 2. Temporal evolution of droplet impact ferrohydrodynamics for different Bo_m for (a) P0–F2.5, (b) P5–F2.5, and (c) P10–F2.5 fluids. The figure shows the role of increasing non-Newtonian fluid nature on the droplet impact ferrohydrodynamics. The scale bars represent 2.8 mm. The images are 1.6 ms apart. The magnetic field acts along the x -direction [coordinate axis is shown in the first row, first column of (c)].

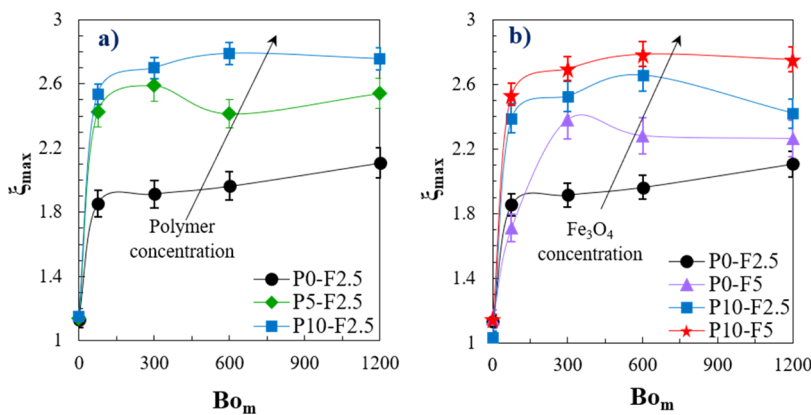


Figure 3. Effect of magnetic Bond number (Bo_m) on the maximum non-dimensional orthogonal spreading (ξ_{max}) with (a) varying polymer concentrations and (b) magnetic particle concentrations.

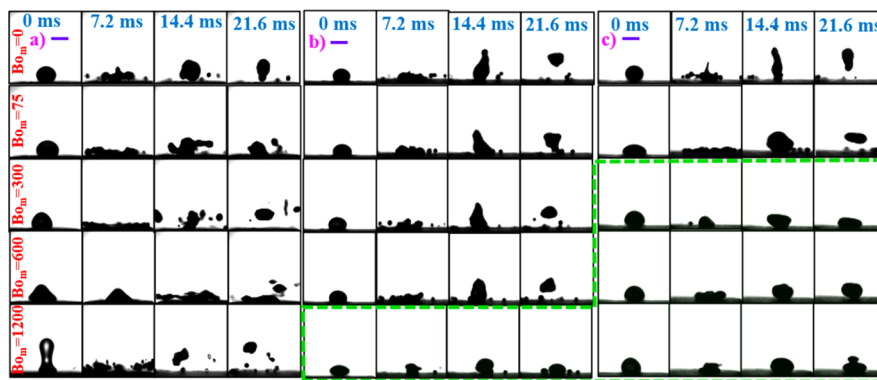


Figure 4. Effects of polymer concentrations on the rebound kinetics of the ferrofluid droplets over the SH surface for different magnetic Bond numbers at $We \sim 100$ for (a) P0-F2.5, (b) P5-F2.5, and (c) P10-F2.5. The scale bars represent 2.8 mm. From top to bottom, the rows represent $Bo_m = 0, 75, 300, 600$, and 1200. The region circumscribed by the dashed lines illustrates the regimes of rebound suppression.

is due to the linear magnetization of the ferrofluid droplet^{23,24} in the low field regime. In a previous report,²⁵ it has been shown that PEG chains may entangle Fe₃O₄ nanoparticles to form a particle–polymer chain mesh. We believe, in the non-Newtonian ferrofluids, the particles entangled to the fluid phase are able to arrest the spread along the x -direction to a greater extent. This is possible as the magnetic force acts on the whole fluid in a more uniform manner compared to the Newtonian case where the particles are dispersed and prone to magnetophoretic drift with respect to the fluid. Consequently, the droplet spreads to a larger extent along the z -direction, thereby increasing the ξ_{max} . At the same time, for a fixed polymer (P10) concentration, ξ_{max} increases with increasing magnetic particle concentrations (Figure 3b).

3.2. Droplet Rebound Suppression Kinetics. In this section, we shall discuss the phenomenology and physical mechanisms responsible for the suppression of rebound of the droplets under the effect of the magnetic field.

3.2.1. Role of Polymer Concentration. The rebound phenomenology of the ferrofluid droplets in the presence of a horizontal uniform magnetic field on SH surfaces has been shown in Figure 4. The set of experiments reported was carried out at a fixed Weber number $We \sim 100$ and magnetic nanoparticle concentration (F2.5), and the figure illustrates the role of polymer concentration (non-Newtonian behavior). Additionally, as a set of control experiments (not illustrated), we performed the impact studies for only polymer solutions (P5-F0 and P10-F0) for different We and Bo_m , and no

rebound suppression is noted at all. It can be readily observed that in the absence of the magnetic field ($Bo_m = 0$), both Newtonian and non-Newtonian ferrofluid droplets exhibit the usual droplet rebound behavior (Figure 4a–c, first row). In the case of Newtonian ferrofluid, increasing the Bo_m reveals the following sequence of droplet impact outcomes, such as spreading, retraction, recoil, rebound, and fragmentation. Under no circumstances, the non-Newtonian ferrofluid exhibits rebound suppression for the studied range of Bo_m (Figure 4a).

Next, we focus on the non-Newtonian ferrofluids and keep the magnetic nanoparticle concentration fixed (F2.5) while varying the polymer concentrations. The lower polymer concentration (P5) ferrofluid droplets also show a similar impact phenomenology as the Newtonian ferrofluid droplets up to $Bo_m \sim 600$ (Figure 4b). However, at higher magnetic field strength ($Bo_m \sim 1200$), onset of rebound suppression of the droplet was observed (Figure 4b, fifth row). In the case of higher polymer concentrations (P10), post-impact stages similar to P0 and P5 ferrofluids are noted in the absence of the magnetic field (Figure 4c 1st row). However interestingly, the P10 ferrofluids exhibit the onset of rebound suppression at a much lower magnetic field strength regime ($Bo_m \sim 300$) (Figure 4c, third row) in comparison to the P5 fluid. For ease of illustration, we have enclosed the paradigms of rebound suppression, as shown in Figure 4 with dashed green lines. Thereby, we infer that at fixed impact We and magnetic particle concentration, the presence of certain non-Newtonian

effects, in conjunction with the magnetic force on the ferrofluid, triggers the rebound suppression phenomenon.

3.2.2. Role of Magnetic Particle Concentration. Next, we probe the role of the magnetic particle concentration, which governs the magnetic force on the ferrofluid at a particular magnetic field (as illustrated in Figure 5). We fix the polymer

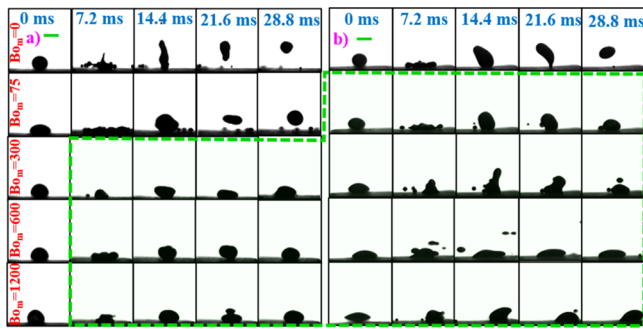


Figure 5. Effects of the magnetic particle concentration on the rebound suppression over the SH surface for different magnetic Bond numbers, for (a) P10-F2.5 and (b) P10-F5, at $We \sim 100$. The scale bar represents 2.81 mm. From top to bottom, the rows represent $Bo_m = 0, 75, 300, 600$, and 1200. The region circumscribed by the dashed lines illustrates the regimes of rebound suppression.

concentration (P10) and the Weber number ($We \sim 100$) and vary the magnetic particle concentration (F2.5 and F5). In the absence of the magnetic field, both the ferrofluid droplets (P10-F2.5 and P10-F5) show the typical rebound nature of SH surfaces (Figure 5a,b, first row). The low concentration (F2.5) non-Newtonian ferrofluid droplet shows the onset of rebound suppression at a moderate $Bo_m \sim 300$. However, in the case of a high concentration ferrofluid (F5), the same is noted at $Bo_m \sim 75$. Our control experiments using Newtonian ferrofluid droplets of F2.5 (Figure 4a) and F5 do not show any such rebound suppression events, even at $Bo_m \sim 1200$. Hence from the observations, we may further infer that the rebound suppression event is triggered by interplay of the magnetic and the non-Newtonian effects in the presence of a magnetic field. Compared to P10-F2.5, the droplet of higher magnetic particle concentration (P10-F5) exhibits fragmentation into secondary droplets during receding and subsequent rebound inhibition. In the case of P10-F5 drops, the magnetic force induced is greater (due to higher magnetic particle population) than P0-F2.5. The higher magnetic force overpowers the interfacial energy, leading to the breakage of finger-like elements attached to the central portion from the main drop.

3.2.3. Role of Impact Weber Number. In this section, we discuss the role of the impact We . The impact phenomenology of different non-Newtonian ferrofluid droplets at two different $We \sim 40$ and ~ 100 have been illustrated in Figure 6. Our experiments show (not illustrated) that when the polymer concentration is kept constant and magnetic particle concentration varied, the onset of rebound suppression under magnetic field influence is not governed by the We . However, the same is not true for the case where the magnetic particle concentration is kept fixed, and the polymer concentration varied (Figure 6). At a fixed $We \sim 40$, irrespective of the nature of the ferrofluid (Newtonian or non-Newtonian) and the Bo_m , the droplets do not exhibit any sign of rebound suppression. When the same set of impact experiments are conducted at $We \sim 100$, we note significant

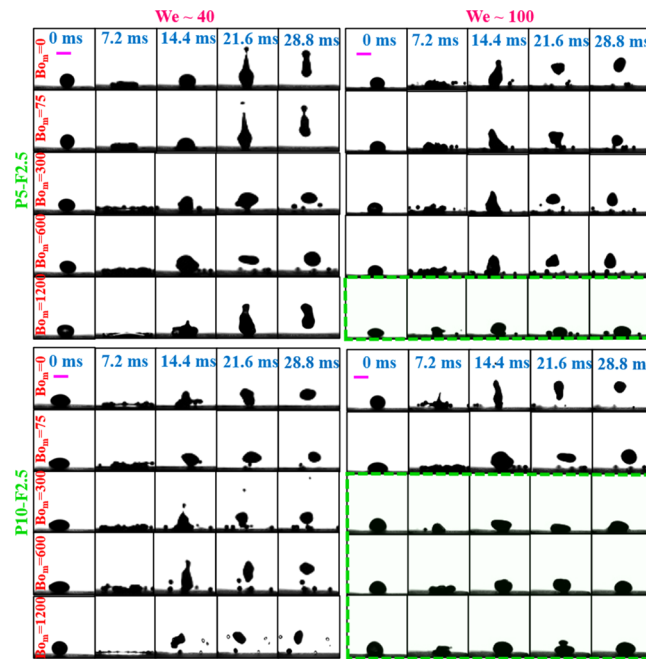


Figure 6. Effects of the impact Weber number on the impact events over SH surfaces for different Bo_m at $We \sim 40$ and ~ 100 . The scale bar represents 2.81 mm. From top to bottom, the rows represent $Bo_m = 0, 75, 300, 600$, and 1200. The regions circumscribed by the dashed lines illustrate the regimes of rebound suppression.

and drastic change in the associated hydrodynamics. At higher We , the onset of rebound suppression is observed at $Bo_m \sim 1200$ for low polymer concentration (P5) and at $Bo_m \sim 75$ for high polymer concentration (P10) cases. We therefore infer that the impact We and the non-Newtonian characteristics of the fluid (polymer concentration) also interplay, and higher We leads to the triggering of the magneto-elastic effect. This observation is in agreement with our previous report on the elastic instability in non-Newtonian droplets.¹³

3.2.4. "Magneto-Elastic" Effect and Role of Magnetic Weissenberg Number. From the discussion in the previous three subsections, we infer that an interplay of the impact mechanics (manifested through the We , refer Figure 6), the elasticity of the fluid (manifested through the polymer concentration, refer Figure 4), and the ferrohydrodynamic forces (manifested through the Bo_m) are responsible for the triggering of the rebound suppression event. It is evident from Figure 4 that with increasing polymer concentrations, rebound suppression is achieved at much lower Bo_m at a fixed $We \sim 100$. In the absence of polymers (P0-F2.5), even at the highest $Bo_m \sim 1200$, no rebound inhibition was observed. On the other hand, for P5-F2.5 and P10-F2.5, the Bo_m at which the rebound suppression was observed was 1200 and 300, respectively. Clearly with increasing polymer concentrations, the non-Newtonian effects are triggering the onset of rebound suppression at lower Bo_m . From Figure 6, it was observed that for a fixed magnetic particle concentration, with increasing Weber number, the critical Bo_m for the rebound suppression is reduced. Therefore, it is evident that the non-Newtonian effects responsible for droplet rebound suppression^{10,12–14} are becoming more potent with the increase of polymer concentrations as well as We . In this context, it is worthwhile to mention that the relaxation time of the polymeric fluids increase with the polymer concentration. The role of We in

setting up the critical shear rate required for non-Newtonian dynamics to be strong enough to slow down the retraction dynamics of the droplets during retraction is also well documented in earlier studies.^{10,12–14} Now the product of the relaxation time and the shear rate (inverse of the flow time scale) is the classical Wi . Clearly, any phenomenon governed by Wi can be referred as elastic effects.^{31,32} The present study is also focusing the modulation of drop impact dynamics due to varying magnetic field strengths (varying Bo_m). Since the suppression of drop rebound behavior is simultaneously affected by elastic- and magnetic field-induced effects, the onset of droplet rebound was dubbed as the manifestation of “magneto-elastic” instability.

It is at this instance that the plausible role of viscosity of the fluids on the rebound suppression dynamics needs to be discussed. In our previous reports^{13,14} on elastic fluids, we have shown conclusively that the increase in viscosity of the fluids due to the presence of polymer may alter the impact hydrodynamics but does not trigger rebound suppression under any circumstances. In the present study, we have performed detailed rheology and magneto-rheology to understand the role played by viscosity (Figure S3, *Supporting Information*). As a representative case, we shall discuss the case for fluids P5–F2.5 at 0.1 T (corresponding to $Bo_m \sim 600$) and P10–F2.5 at 0 T ($Bo_m = 0$). From the magnetorheology studies, we have observed that the shear viscosities of these two fluids are within 3% of one another (for shear range of 0–300 s⁻¹). Next, we focus on the impact of these two fluids at $We \sim 100$ (Figure 6). Despite the similar viscosities, the P5–F2.5 exhibits rebound suppression at $Bo_m \sim 600$, whereas the P10–F2.5 exhibit the typical rebound of SH surfaces at $Bo_m \sim 0$. This clearly illustrates that the rebound suppression is not triggered by the increase in the viscosity of the ferrofluids due to the magnetorheological effect, and there is some other non-trivial mechanism at play.

For the explanation, we appeal to our previous report on rebound suppression of elastic fluid droplets on SH surfaces and the references within.¹³ We showed that using very dilute PAM solution droplets, it was possible to induce elastic instability during the retraction phase after impact, which led to rebound suppression. During the spreading phase of the droplet, the long polymer chains unwind due to shear at the spreading contact line, and similar observations have been reported in the literature.¹² During the retraction phase, the polymer chains recoil, and the recoiling dynamics is governed by the relaxation timescale of the polymer molecules. If the concentration of the polymer in the solution is such that the relaxation timescale of the non-Newtonian fluid is smaller than the timescale of retraction of the contact line, then the retracting contact line is not subjected to the normal stress generated against the retraction. In such cases, the droplet rebounds as typical on SH surfaces. In the event, the polymer concentration is above the threshold, such that the relaxation timescale is greater than the retraction timescale, the triple line retracts faster than the polymer chains, leading to a normal stress generation which decelerates the retraction velocity. In the absence of high retraction velocity, the rebound is suppressed. We have also shown that for all such cases of rebound suppression, the associated Weissenberg number ($Wi = \lambda\dot{\gamma}$, where λ is the relaxation time of the fluid, and $\dot{\gamma}$ is the shear rate at onset of retraction) is always greater than one. This signifies that the event is triggered by elastic instability within the fluid.¹³ As the impact We increases, the retraction

shear rate increases, and the droplets show higher propensity of rebound arrest. Needless to say, there may be an upper bound to the Weber number beyond which the drops may fragment upon impact on the ground. The present experimental study is performed at the Weber number well below this upper bound.

At this juncture, it is noteworthy that such elastic instability can only be triggered in the case of very long-chain polymer molecules. In the present study, we have used PEG-400, which is a very short-chain polymer, and thus, the droplets cannot exhibit rebound suppression (via the route of elastic instability) for the range of impact We explored. We further confirm this using theoretical analysis and control experiments on the polymer solutions and non-Newtonian ferrofluids in the absence of the field. In the previous report,¹³ we have noted that for all cases of rebound suppression, $Wi > 1$ is satisfied signifying the onset of elastic instability. Following the same methodology, we deduce the approximate shear rates at the termination of the spreading regime and onset of the retraction regime from image processing. To determine the relaxation timescales for the polymer solutions, we take the aid of oscillatory rheometry. We first determine the viscoelastic signatures of the polymer solutions and non-Newtonian ferrofluids and obtain the elastic (G') and viscous (G'') moduli of the fluids as a function of oscillatory frequency (ω). From the viscoelastic response, we obtain the approximate relaxation times for the different fluids based on established theories.^{26–28} While employing the theoretical framework to deduce the relaxation timescales for the non-Newtonian ferrofluids, we have assumed that the nanoparticle-based polymer solutions also conform to a similar viscoelastic model as the polymer solutions.

Based on the shear rates and relaxation timescales, we determine the Wi and observe that all the values (for different impact We) are well below one. This signifies that the elastic instability is absent in the droplets of only polymer solution and the non-Newtonian ferrofluids in the absence of field. We have already ruled out the role of increased viscosity under the magnetic field as a possible governing agent. Furthermore, we have also noted that there is no rebound suppression in the absence of field. Thereby, all evidences lead to the inference that a conjugate effect between the elastic and the magnetic forces is occurring, which leads to the rebound suppression. Next, we apply the same methodology to the different cases of non-Newtonian ferrofluid droplets impacting under the field effect. To determine the relaxation timescales under the effect of one particular field strength, we perform frequency sweep oscillatory magnetorheology experiments at different field strengths (Figure S4, *Supporting Information*) and employ the methodology reported previously.^{13,14} We determine the values of the Wi for different impact velocity and magnetic field strength cases (here we use magnetic field strength instead of Bo_m as the wide range of properties in the presence of field does not allow for the use of a single specific Bo_m value). Although the Wi values are greater than the zero-field cases, it is noted that the values of the Wi even for the cases of field-induced rebound suppression are below one.

As the Wi cannot provide a valid physical picture of the proposed magneto-elastic effect, we propose a modified form of the non-dimensional number to incorporate the effects of the magnetic field. Based on the experimental observations, we propose a new non-dimensional variable, which we term as the magnetic Weissenberg number, expressed as $Wi_m = Wi^{1/2}Bo_m^2$.

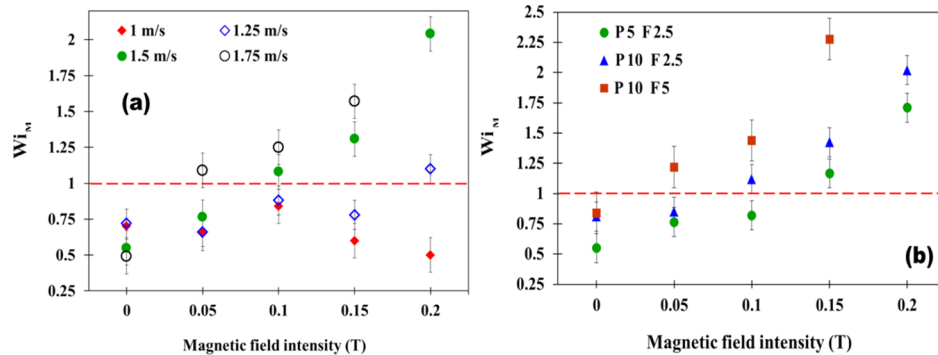


Figure 7. Plot of the magnetic Weissenberg number (Wi_m) against the magnetic field intensity, for (a) P10-F2.5 droplets impacting at different velocities and (b) for different non-Newtonian ferrofluid droplets impacting at a velocity of 1.5 m/s. The horizontal dashed line indicated $Wi_m = 1$. All points lying in the regime above this line exhibit rebound suppression triggered by the magneto-elastic effect.

Physically, the number is the ratio of the magneto-elastic forces to the visco-capillary forces within the non-Newtonian fluid, and we believe that it will be an improved non-dimensional number which shall be able to incorporate the magnetic effects within the gamut of the Wi . The exponents for Wi and Bo_m in the expression for Wi_m are based on the detailed experimental data, and we have selected them in a manner such that the onset of magneto-elastic effect-induced rebound suppression happens at the value of 1. The values of Wi_m for P10-F2.5 droplets for different impact velocities and different magnetic field strengths have been illustrated in Figure 7a. We observe that the magnetic Weissenberg number criterion is able to segregate the regimes of rebound and rebound suppression ($Wi_m > 1$), with respect to both the impact velocity and applied magnetic field strength. The behavior of the Wi_m with respect to the magnetic field strength for different non-Newtonian ferrofluid droplets impacting the SH surface at 1.5 m/s has been illustrated in Figure 7b. It can be seen that the proposed Wi_m is able to predict the paradigm of rebound suppression for different non-Newtonian ferrofluids. From the innate definition of the Wi_m and the fact that we can consistently predict rebound suppression at $Wi_m > 1$, our hypothesis on the presence of magneto-elastic effects in non-Newtonian ferrofluid impact dynamics is further cemented. Physically, Figure 7 highlights that for a given magnetic field strength, both polymer concentration and high impact velocity are essential to trigger the magnetic elastic effects to be dominant enough to cause rebound suppression. It must be noted that addition of polymers triggers the onset of instability at much lower Bo_m in comparison to the Newtonian counterpart (see Figure 4). Hence, for a low polymer concentration fluid, at a given Bo_m , higher Weber number (higher impact velocity) is required to reach the critical shear rate required for non-Newtonian effects to be dominant in slowing down the retraction velocity. On the other hand, for the same Bo_m , for a high concentration polymer droplet, comparatively lower impact velocity (lower Weber number) is required to trigger the magneto-elastic effects.

3.3. Droplet Ferrohydrodynamic Regimes. In this section, we elucidate various impact ferrohydrodynamic regimes of non-Newtonian ferrofluid droplets in the presence of external uniform horizontal magnetic field. As evident from Figure 8, although the regime maps of the various drop impact outcomes for the three different test fluids (P5-F2.5, P10-F2.5, and P10-F5) are seemingly different from each other, we have tried to highlight the common features in the discussion

of the five regimes, as represented in Figure 8. The regime maps for We versus Bo_m and magnetic capillary number (Ca_m) versus Hartmann number (Ha) for different ferrofluids have been illustrated in Figure 8. In this study, the effect of We , Bo_m , and magnetic particle concentration was not sufficient to emphasize the impact hydrodynamic outcomes like breakup during retraction and rebound inhibition. The physical insights on the effect of relative dominance of magnetic force to viscous force and relative dominance of viscous force to surface tension force are also needed to explain the rebound suppression phenomenon of non-Newtonian ferrofluid droplets. Hence, we have additionally introduced the Ca_m and Ha to predict the capillary-driven hydrodynamic outcomes such as, breakup during retraction (receding breakup), and rebound suppression (at the phase map section).

We discuss the various regimes in the phase map as follows

Regime-0 (non-experimental regime): In this regime, the needle and droplet assembly lie within the direct influence of magnetic poles. The growing droplet is pulled away from the needle by the magnetic field and distorted largely before the impact, which does not lead to physically consistent observations. Thereby, experiments have not been performed in this regime. For all the test fluids, this regime was observed for low We and low Ca , irrespective of Bo_m and Ha .

Regime-I (rebound with pinch-off): In this regime, the droplet rebounds with pinch-off (releasing a tiny droplet from the rebounding parent droplet). This rebound with pinch-off behavior exists due to the dominance of the inertial and capillary forces compared to the magnetic force. Accordingly, this regime is noted to occur at low Bo_m where the magnetic forces are weak, and at low to moderate We such that the impact process does not lead to shattering of the droplet due to high inertia.

Regime-II (complete rebound): Complete rebound takes place in this regime, due to the dominance of recoil kinetic energy of the droplet over viscous dissipation during spreading and the magnetic body force. However in this regime, the capillary force is overshadowed by the rebound inertia, and pinch-off is absent. We presume that at relatively higher We , non-Newtonian effects are sufficiently strong to suppress the capillary instability-induced pinch-off. Consequently, the regime appears in close conjunction with R-I but extends to relatively higher We .

If we club the regimes I and II as just the rebound effect, it is evident that these two regimes are occurring in the bottom left corner above regime 0 of the regime maps, that is, for low We

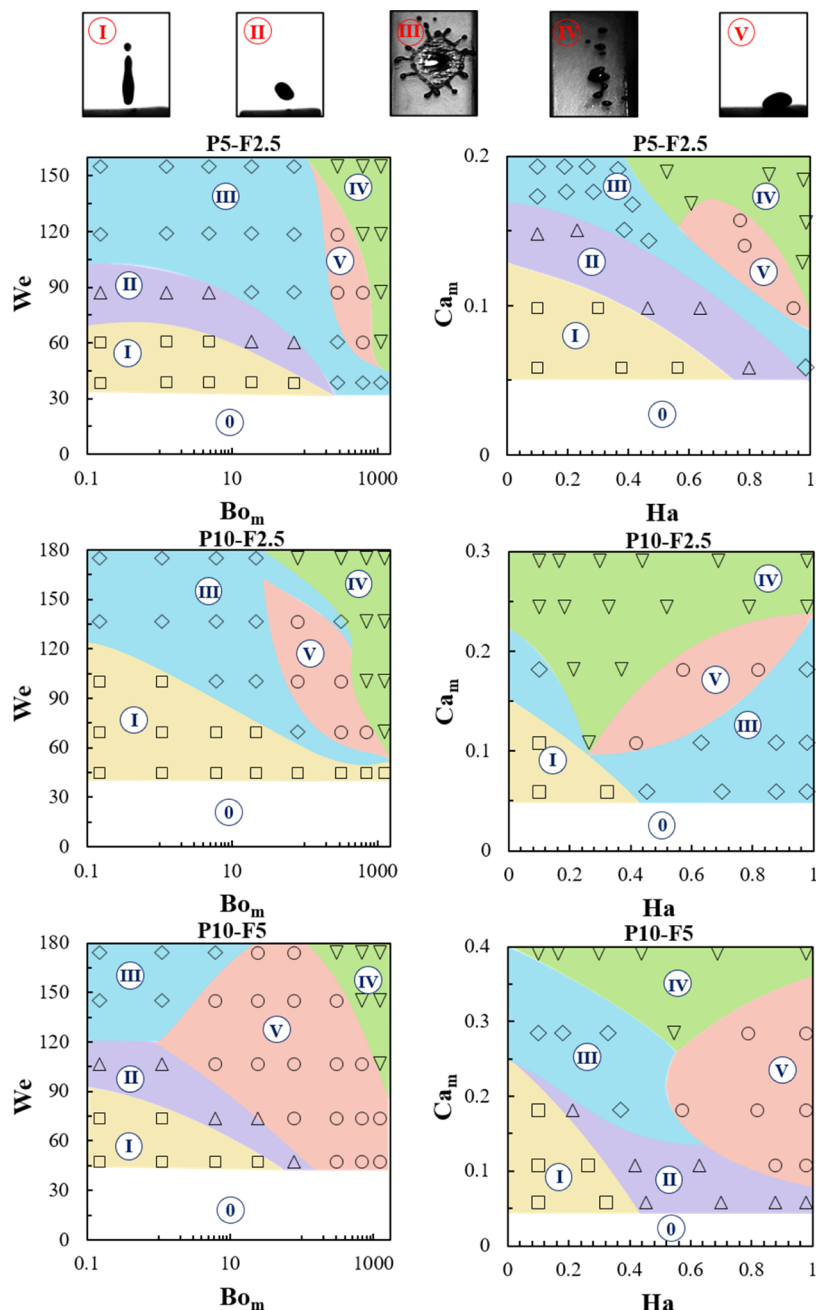


Figure 8. Phase maps indicating the different impact ferrohydrodynamic outcomes of non-Newtonian ferrofluid droplets in magnetic field ambience. The regimes 0, I, II, III, IV, and V represent “non-experimental regime,” “rebound with pinch-off,” “complete rebound,” “breakup during retraction,” “fragmentation” (with orthogonal elongation), and “rebound suppression,” respectively. Additional information is provided in Figure S7 (Supporting Information).

and low Ca . Low impact height is a prerequisite for the rebound event of non-Newtonian ferrofluid droplets. We have tried to establish the scaling relationship of the rebound regime (RI and R II combined) from the non-rebound regime in the form of $We \sim a(Bo_m)^{-b}$, where a is the prefactor and b is the power law exponent (refer Figures S5 and S6 for the detailed fitting analysis). The power law exponents are approximately -0.123 , -0.125 , and -0.143 for the P5-F2.5, P10-F2.5, and P10-F5, respectively.

Regime-III (breakup during retraction): The droplet breaks up during the retraction stage in this regime.²⁹ In this regime, the droplet spreads to its maximum spread state and forms radial filaments, which do not detach immediately as the

capillary forces are dominated by the viscoelasticity of the fluid. The formation of the secondary droplets attached to the rim by thin filaments is referred as prompt splash.³⁰ At the maximum spread state, the magnetic force on the bulbs at the ends of the filaments is high at even moderate Bo_m . During the retraction stage, the recoil inertia is overcome by the magnetic force, and the bulbs detach off the retracting parent droplet to form smaller droplets. This regime occurs at higher We and moderate Bo_m as higher inertia ensures the maximum spread state, and the moderate Bo_m ensures the detachment of the filamentous droplets at retraction. For P5-F2.5 and P10-F2.5, this regime is observed starting from the top left corner (high We and low Bo_m) extending up to the bottom right corner (low

We and high Bo_m). However for P10–F5, this regime is only limited to the top corner due to the occurrence of rebound suppression (regime V) for a broader range of We and Bo_m .

Regime-IV (fragmentation): Fragmentation of the droplet into smaller secondary droplets occurs in this regime. This occurs at either high We or high Bo_m . At high We, the impact inertia is high enough to induce fragmentation of the droplet during the spreading state, caused by formation of large velocity gradients within the spreading droplet, which overcomes the capillary and viscous forces. At high Bo_m , the magnetic force on the spreading droplet is high enough to induce ferrohydrodynamic instability,⁹ which leads to rupturing of the spreading droplet as the magnetic forces overcome the capillary forces.

Regime-V (rebound suppression): In this regime, suppression of droplet rebound takes place due to the magneto-elastic instability, already explained in the preceding section. The requirement of the magneto-elastic instability to occur, that is, $Wi_m = Wi^{1/2}Bo_m^2 > 1$, is ensured when the combined effect of We and Bo_m is sufficient to trigger the instability. This occurs at the junctions of R-III and R-IV, where the We is moderate enough to induce the elastic instability during the retraction process, and the Bo_m is moderate enough to induce the optimum ferrohydrodynamic force on the droplet. For the P5–F2.5 and P10–F2.5, the regime is sandwiched between regime III and IV. For the same particle concentrations (F2.5), the higher polymer concentration fluid P10–F2.5 has broader area of regime V than P5–F2.5. As evident from Figure 8, bottom row, the extent of the regime increases in size to a much greater extent in the case of P10–F5, that is, with increase in the elasticity of the fluid (polymer concentration) and magnetic moment of the droplet (magnetic particle concentration).

In previous studies of drop impact on hydrophobic surfaces in the absence of the magnetic field,^{31,32} it was observed that the impact outcome varies from deposition (no rebound), partial rebound, complete rebound, and finally fragmentation with the increasing We. Since our experimental study is incorporating the features of non-Newtonian effects and magnetic field, the impact outcomes are strikingly different with the increase of We. In our case, at the lowest We, rebound is observed, and at higher We drop, rebound is suppressed. In addition, with increase of Bo_m , even at the lower range of We rebound suppression was observed especially in the case of P10–F5 (Figure 8, bottom row, left column). For a detailed regime map showing the role of We and Bo_m , and the segregation of the regimes based on the impact behavior and magnetic field constraints, refer Figure S7 (Supporting Information).

4. CONCLUSIONS

In this study, we report an extensive experimental investigation on the impact ferrohydrodynamics of non-Newtonian ferrofluid droplets on the SH surface in the presence of a horizontal uniform magnetic field. We used stable colloidal solutions of magnetic nanoparticles dispersed in polymeric solutions as the non-Newtonian ferrofluids. The studies encompass a range of impact We up to ~180 and $Bo_m \sim 0$ –1500. We noted that in the presence of the magnetic field, the non-dimensional maximum spreading (ξ_{max}) increases compared to the Newtonian ferrofluids with increasing both polymer and magnetic particle concentrations. Through experimental investigations, we have studied the effects of

polymer concentration, magnetic nanoparticle concentration, Weber number, and Bo_m on the impact dynamics of non-Newtonian ferrofluid droplet. Addition of polymers to the base Newtonian ferrofluid caused rebound suppression at lower Bo_m for fixed magnetic particle concentration and We. Similarly for fixed polymer concentration and We, increase of magnetic particle concentration triggered rebound suppression at lower Bo_m .

The combined effect of magnetic particles and elastic effects of polymer chains, together clubbed as magneto-elastic effects, similar to the coinage of the elasto-inertial effect of earlier studies^{13,33} is shown to be responsible for the early onset of rebound suppression. We formed a non-dimensional number termed as magnetic Weissenberg number, Wi_m taking into account of the effect of classical Weissenberg number and the magnetic Bond number. Through the scaling analysis we showed that when $Wi_m \geq 1$ magneto-elastic instability is triggered and droplet rebound suppression is observed for the first time. This is analogous to the situations when purely elastic instability sets in^{34,35} or onset of drag reduction³⁶ for $Wi \geq 1$. Finally, ferrohydrodynamics of non-Newtonian ferrofluid droplet behavior regime phase maps over a wide range of corresponding dimensionless numbers such as We, Bo_m , Ca_m , and Ha were presented. The present findings may have significant implications toward design and development of micro or macroscale systems and devices involving magnetic liquid droplets.

■ ASSOCIATED CONTENT

SI Supporting Information

The Supporting Information is available free of charge at <https://pubs.acs.org/doi/10.1021/acs.langmuir.1c00885>.

Physical properties of the ferrofluids, additional data on experimental setup, data on their rheology, viscoelastic behavior, and so forth (PDF)

■ AUTHOR INFORMATION

Corresponding Authors

Purbarun Dhar – Department of Mechanical Engineering, Indian Institute of Technology Kharagpur, Kharagpur 721302 West Bengal, India; orcid.org/0000-0001-5473-2993; Phone: +91-3222-28-2938; Email: purbarun@mech.iitkgp.ac.in, purbarun.iit@gmail.com

Devrjanan Samanta – Department of Mechanical Engineering, Indian Institute of Technology Ropar, Rupnagar 140001 Punjab, India; Phone: +91-1881-24-2109; Email: devranjan.samanta@iitrpr.ac.in

Author

Gudlavalleti V V S Vara Prasad – Department of Mechanical Engineering, Indian Institute of Technology Ropar, Rupnagar 140001 Punjab, India

Complete contact information is available at: <https://pubs.acs.org/10.1021/acs.langmuir.1c00885>

Notes

The authors declare no competing financial interest.

■ ACKNOWLEDGMENTS

G.V.V.S.V.P. would like to thank the Ministry of Education, Government of India, for the doctoral scholarship. D.S. would like to thank IIT Ropar for partially funding the work (vide

grant 9-246/2016/IITRPR/144). P.D. thanks IIT Kharagpur (vide grant SFI) and Science and Engineering Research Board (SERB) (vide grant SRG/2020/000004) for partially funding the work.

■ REFERENCES

- (1) Yarin, A. L. DROP IMPACT DYNAMICS: Splashing, Spreading, Receding, Bouncing. *Annu. Rev. Fluid Mech.* **2006**, *38*, 159–192.
- (2) Almohammadi, H.; Amirkazli, A. Asymmetric Spreading of a Drop upon Impact onto a Surface. *Langmuir* **2017**, *33*, 5957–5964.
- (3) Visser, C. W.; Pohl, R.; Sun, C.; Römer, G.-W.; Huis in 't Veld, B.; Lohse, D. Toward 3D Printing of Pure Metals by Laser-Induced Forward Transfer. *Adv. Mater.* **2015**, *27*, 4087–4092.
- (4) Gijs, M. A. M.; Lacharme, F.; Lehmann, U. Microfluidic applications of magnetic particles for biological analysis and catalysis. *Chem. Rev.* **2010**, *110*, 1518–1563.
- (5) Ahmed, A.; Fleck, B. A.; Waghmare, P. R. Maximum spreading of a ferrofluid droplet under the effect of magnetic field. *Phys. Fluids* **2018**, *30*, 077102.
- (6) Sudo, S.; Wakamatsu, N.; Ikohagi, T.; Nishiyama, H.; Ohaba, M.; Katagiri, K. Magnetic field effects in the impact of a magnetic fluid drop. *J. Magn. Magn. Mater.* **1999**, *201*, 285–289.
- (7) Rahimi, S.; Weihl, D. Experimental investigation of magneto-rheological droplet impact on a smooth surface. *J. Magn. Magn. Mater.* **2009**, *321*, 3178–3182.
- (8) Zhou, J.; Jing, D. Effects of vertical magnetic field on impact dynamics of ferrofluid droplet onto a rigid substrate. *Phys. Rev. Fluids* **2019**, *4*, 83602.
- (9) Sahoo, N.; Khurana, G.; Samanta, D.; Dhar, P. Collisional ferrohydrodynamics of magnetic fluid droplets on superhydrophobic surfaces. *Phys. Fluids* **2021**, *33*, 012012.
- (10) Bartolo, D.; Boudaoud, A.; Narcy, G.; Bonn, D. Dynamics of non-newtonian droplets. *Phys. Rev. Lett.* **2007**, *99*, 1–4.
- (11) Mao, T.; Kuhn, D. C. S.; Tran, H. Spread and Rebound of Liquid Droplets upon Impact on Flat Surfaces. *AIChE J.* **1997**, *43*, 2169–2179.
- (12) Smith, M. I.; Bertola, V. Effect of polymer additives on the wetting of impacting droplets. *Phys. Rev. Lett.* **2010**, *104*, 1–4.
- (13) Dhar, P.; Mishra, S. R.; Samanta, D. Onset of rebound suppression in non-Newtonian droplets post-impact on superhydrophobic surfaces. *Phys. Rev. Fluids* **2019**, *4*, 103303.
- (14) Dhar, P.; Mishra, S.; Gairola, A.; Samanta, D. Suppressed Leidenfrost phenomenon during impact of elastic fluid droplets. *Proc. R. Soc. A* **2020**, *476*, 20200556.
- (15) Zang, D.; Wang, X.; Geng, X.; Zhang, Y.; Chen, Y. Impact dynamics of droplets with silica nanoparticles and polymer additives. *Soft Matter* **2013**, *9*, 394–400.
- (16) Yun, S.; Hong, J.; Kang, K. H. Suppressing drop rebound by electrically driven shape distortion. *Phys. Rev. E: Stat., Nonlinear, Soft Matter Phys.* **2013**, *87*, 1–5.
- (17) Yun, S.; Lim, G. Ellipsoidal drop impact on a solid surface for rebound suppression. *J. Fluid Mech.* **2014**, *752*, 266–281.
- (18) Antonini, C.; Villa, F.; Bernagozzi, I.; Amirkazli, A.; Marengo, M. Drop rebound after impact: The role of the receding contact angle. *Langmuir* **2013**, *29*, 16045–16050.
- (19) Pack, M. Y.; Yang, A.; Perazzo, A.; Qin, B.; Stone, H. A. Role of extensional rheology on droplet bouncing. *Phys. Rev. Fluids* **2019**, *4*, 1–11.
- (20) Jaiswal, V.; Dwivedi, R. K.; Harikrishnan, A. R.; Dhar, P. Magnetohydrodynamics- and magnetosolutal-transport-mediated evaporation dynamics in paramagnetic pendant droplets under field stimulus. *Phys. Rev. E* **2018**, *98*, 13109.
- (21) Katiyar, A.; Dhar, P.; Nandi, T.; Das, S. K. Magnetic field induced augmented thermal conduction phenomenon in magneto-nanocolloids. *J. Magn. Magn. Mater.* **2016**, *419*, 588–599.
- (22) Sahoo, N.; Khurana, G.; Harikrishnan, A. R.; Samanta, D.; Dhar, P. Post impact droplet hydrodynamics on inclined planes of variant wettabilities. *Eur. J. Mech. B/Fluids* **2020**, *79*, 27–37.
- (23) Cui, G.; Jacobi, I. Magnetic Control of Ferrofluid Droplet Adhesion in Shear Flow and on Inclined Surfaces. *Langmuir* **2020**, *36*, 10885–10891.
- (24) Rigoni, C.; Bertoldo, S.; Pierino, M.; Talbot, D.; Abou-Hassan, A.; Mistura, G. Division of Ferrofluid Drops Induced by a Magnetic Field. *Langmuir* **2018**, *34*, 9762–9767.
- (25) Katiyar, A.; Dhar, P.; Das, S. K.; Nandi, T. Near-field magnetostatics and Néel-Brownian interactions mediated magneto-rheological characteristics of highly stable nano-ferrocolloids. *Soft Matter* **2015**, *11*, 1614–1627.
- (26) Zhao, Z.; Ji, X.; Dimova, R.; Lipowsky, R.; Liu, Y. Viscoelasticity of poly(ethylene glycol) solutions on supported lipid bilayers via quartz crystal microbalance with dissipation. *Macromolecules* **2015**, *48*, 1824–1831.
- (27) Shi, X.; Kenney, S.; Chapagain, G.; Christopher, G. F. Mechanisms of onset for moderate Mach number instabilities of viscoelastic flows around confined cylinders. *Rheol. Acta* **2015**, *54*, 805–815.
- (28) Tirtaatmadja, V.; McKinley, G. H.; Cooper-White, J. J. Drop formation and breakup of low viscosity elastic fluids: Effects of molecular weight and concentration. *Phys. Fluids* **2006**, *18*, 043101.
- (29) Grishaev, V.; Iorio, C. S.; Dubois, F.; Amirkazli, A. Complex Drop Impact Morphology. *Langmuir* **2015**, *31*, 9833–9844.
- (30) Rioboo, R.; Tropea, C.; Marengo, M. Drop impact on solid surfaces. *Atomization Sprays* **2001**, *11*, 12.
- (31) Kim, H.; Lee, C.; Kim, M. H.; Kim, J. Drop Impact Characteristics and Structure Effects of Hydrophobic Surfaces with micro and or nanoscaled structures. *Langmuir* **2012**, *28*, 11250–11257.
- (32) Guo, C. Drop impact on Anisotropic Superhydrophobic surfaces. *Langmuir* **2018**, *34*, 3533–3540.
- (33) Samanta, D. Elasto-inertial turbulence. *Proc. Natl. Acad. Sci. U.S.A.* **2013**, *110*, 10557–10562.
- (34) Larson, R. G.; Shaqfeh, E. S. G.; Muller, S. J. A purely elastic instability in Taylor–Couette flow. *J. Fluid Mech.* **1990**, *218*, 573.
- (35) Shaqfeh, E. S. G. Purely Elastic Instabilities in Viscometric Flows. *Annu. Rev. Fluid. Mech.* **1996**, *28*, 129–185.
- (36) White, C. M.; Mungal, M. G. Mechanics and Prediction of Turbulent Drag Reduction with Polymer Additives. *Annu. Rev. Fluid Mech.* **2008**, *40*, 235–256.